

## Article

# Pseudo-Stilbene- and Azobenzene-Type Systems for Optical Frequency Conversion: Estimating the First-Order Molecular Hyperpolarizability

Raiane S. Araújo<sup>1</sup>, José J. Rodrigues, Jr.<sup>2</sup> , Márcio A. R. C. Alencar<sup>2</sup> , Jamal Rafique<sup>3,4</sup> , Sumbal Saba<sup>3</sup>  and Luis M. G. Abegão<sup>5,\*</sup> 

<sup>1</sup> School of Engineering, Mackenzie Presbyterian University, São Paulo 01302-907, SP, Brazil

<sup>2</sup> Department of Physics, Federal University of Sergipe, São Cristóvão 49100-000, SE, Brazil; joatan@academico.ufs.br (J.J.R.J.); marcalencarufs@academico.ufs.br (M.A.R.C.A.)

<sup>3</sup> Sustainable Synthesis and Organochalcogen Laboratory, Institute of Chemistry, Federal University of Goiás, Goiânia 74690-900, GO, Brazil; sumbalsaba@ufg.br (S.S.)

<sup>4</sup> Institute of Chemistry, Federal University of Mato Grosso do Sul, Campo Grande 79074-460, MS, Brazil

<sup>5</sup> Photonics Group, Institute of Physics, Federal University of Goiás, Goiânia 74690-900, GO, Brazil

\* Correspondence: luis.abegao@ufg.br

**Abstract:** This study investigates the potential of a set of pseudo-stilbene and azobenzene molecular structures to become optical frequency converters for optical communications based on a detailed exploration of the first-order molecular hyperpolarizability ( $\beta_{HRS}$ ), which is the microscopic counterpart of second harmonic generation (SHG).  $\beta_{HRS}$  values were obtained via quantum chemical calculations using the Gaussian 16 software package in solvent and gas-phase media at different wavelengths, i.e., 1064 nm, 1310 nm, and 1510 nm. The latter two wavelengths are of particular interest for optical communications. Our study focused on discerning how the molecular structure influences the  $\beta_{HRS}$  response, explicitly highlighting the influence of the azomethine group (CH=N). The results revealed that the molecular planarity, affected by this group, plays a crucial role in modulating the optical properties. The highest  $\beta_{HRS}$  value in a solvent medium using the CAM-B3LYP/6-311+G(2d,p) level of theory achieved in this work was around  $1400 \times 10^{-30} \text{cm}^4 \text{startvolt}^{-1}$ , four orders of magnitude higher than KDP ( $0.2 \times 10^{-30} \text{cm}^4 \text{startvolt}^{-1}$ ), which is a reference in SHG experiments at 1064 nm. The highest calculated  $\beta_{HRS}$  value at the same level of theory and solvent at 1310 nm and 1550 nm was  $631 \times 10^{-30} \text{cm}^4 \text{startvolt}^{-1}$  and  $456 \times 10^{-30} \text{cm}^4 \text{startvolt}^{-1}$ , respectively. All these values belong to molecular structures with azo-coupling with donor (4-NMe<sub>2</sub>) and acceptor (4'-NO<sub>2</sub>) peripheral groups, designated as AB-3.

**Keywords:** pseudo-stilbene and azobenzene; nonlinear optics; second harmonic generation; first-order molecular hyperpolarizability; optical frequency converters; quantum chemical calculations



**Citation:** Araújo, R.S.; Rodrigues, J.J., Jr.; Alencar, M.A.R.C.; Rafique, J.; Saba, S.; Abegão, L.M.G. Pseudo-Stilbene- and Azobenzene-Type Systems for Optical Frequency Conversion: Estimating the First-Order Molecular Hyperpolarizability. *Photonics* **2024**, *11*, 283. <https://doi.org/10.3390/photonics11030283>

Received: 21 February 2024

Revised: 11 March 2024

Accepted: 18 March 2024

Published: 21 March 2024



**Copyright:** © 2024 by the authors. Licensee MDPI, Basel, Switzerland. This article is an open access article distributed under the terms and conditions of the Creative Commons Attribution (CC BY) license (<https://creativecommons.org/licenses/by/4.0/>).

## 1. Introduction

Photonics is a well-established field, transversing various science and technology domains, such as optical communications [1,2]. Since 2020, internet traffic has rocketed, mainly due to the increase in many digital activities because of the lockdowns and restrictions provoked by the coronavirus pandemic [3]. In telecommunications, the broadband concept means wide bandwidth data transmission that transports multiple signals at a wide range of frequencies. Suppose such a signal is an optical rather than an electric signal. In this case, a photonic device that converts the light frequency, i.e., an optical frequency converter (OFC), is essential to increase the optical communications broadband. To choose a material to be used in developing an OFC, firstly, we need to characterize it in terms of nonlinear optics (NLO) [4], particularly by estimating the second harmonic generation (SHG) phenomenon [5]. In other words, we need to assess the material's ability to double the frequency of incident light. Several materials can generate SHG efficiently [6–11],

but organic compounds are best suited for optical communications due to their intrinsic ultra-fast polarization response. In fact, optical nonlinearities, such as optical switching and regeneration, can provide a massive speed advantage over electronic techniques. For example, landmark experiments have reported all-optical switching at well over Terabaud rates [12]. Therefore, fundamental research to understand the SHG response of organic materials is crucial to developing novel OFC.

Numerous organic materials have already investigated [13–18], but the search for novel or modified organic molecular structures with significant NLO responses continues. However, attempting to synthesize a novel molecular structure may be futile and expensive without prior fundamental research and understanding of its inherent optical properties. Moreover, NLO characterization using ultra-short pulses is costly due to the high-end photonics infrastructure needed. For instance, utilizing the hyper-Rayleigh scattering (HRS) method with a femtosecond laser system stands out as a trusted experimental approach to ascertain the first-order molecular hyperpolarizability in solution, denoted as  $\beta_{HRS}$ . The emanated light from  $\beta_{HRS}$  results in incoherent second harmonic generation (ISHG), a crucial spectroscopic measure when assessing the prospects of a proposed OFC. Conversely, adopting a theoretical strategy, specifically quantum chemical calculations (QCCs), offers a more cost-effective means to estimate  $\beta_{HRS}$ . To illustrate, evaluating the  $\beta_{HRS}$  value for a molecular structure comprising roughly 40 atoms can be completed in under a day with a 16-core setup using the Gaussian software package. This timeframe encompasses the entire spectrum of tasks, from molecular design and optimization to the post-processing of the resulting QCC data. Naturally, the duration can vary based on the chosen theoretical level, as noted in reference [19].

Still, not all organic systems are suitable for exploring NLO properties. Usually, a  $\pi$ -conjugated molecular structure containing an electron donor (D) and an electron acceptor (A) is widely known as a push–pull system (D- $\pi$ -A). These molecular systems have become intensely explored [20–22], and the interaction between groups D and A through a bridge of  $\pi$ -electrons is called intramolecular charge transfer (ICT) [23–25]. For example, when charge transfer occurs between electron-donating and electron-accepting groups connected by a conjugated  $\pi$ -bridge, the chromophore exhibits a significant increase in dipole moment [25]. Thus, the impact of ICT on the optical properties of  $\pi$ -conjugated molecules can be observed by the geometry change, the absorption spectrum, and their dependence on the first-order hyperpolarizabilities of molecules [18,26–29].

Chemically, stilbenes are a common and integral feature of a variety of natural products and synthetic structures. They represent a significant “privileged scaffold” and are also of great interest in medicinal chemistry [30]. These scaffolds are also present in a wide range of molecules which have critical applications in material sciences [31,32]. Considering the biological relevance and importance of stilbenes in material science, many related synthetic structures can be found in the literature, known as pseudo-stilbenes. These structures have 4 and 4' positions of the two azo rings with electron-donating and electron-withdrawing groups at opposite ends of the aromatic system [33], which include azomethines (-CH=N-) [34–37], azobenzenes (-N=N-) [20,38–42], and azo-coupling (-N=N-X-Y-) [26,37,43–45]. Such structures are a well-known class of materials with reported NLO responses due to their potential for applications in photonic devices [46]. Furthermore, these systems have been widely reported experimentally and theoretically due to their interesting physicochemical properties, particularly with excellent values of  $\beta_{HRS}$  [34,45–48]. Thus, new organic materials containing the core of these essential groups with highly delocalized  $\pi$ -electrons and their theoretical calculations play a crucial role in NLO applications [26,29,49].

Encouraged by the preceding works, we have decided to estimate the magnitude of the  $\beta_{HRS}$  of a series of pseudo-stilbenes (PS) and azobenzene-based (AB) compounds. In fact, to the best of our knowledge, only the static first-order molecular hyperpolarizability ( $\beta_0$ ) has been reported [49], but not using the Gaussian software package. Also, we have used the most common wavelengths in the field of optical communications ( $\lambda = 1064$  nm,

1310 nm, and 1550 nm) to establish an empirical correlation for future OFC development. Therefore, in this work, QCCs were carried out at the time-dependent density functional theory (TD-DFT) level to estimate the influence of functional groups on the magnitude of the  $\beta_{HRS}$  using Gaussian 16 and Hyper-QCC [19], which is post-processing software.

## 2. Investigated Compounds

From a synthetic point of view, stilbenes (-CH=CH-) are accessible via organic compound carbon-carbon coupling reactions [50]. On the other hand, pseudo-stilbenes can be prepared from the coupling of two different anilines in the case of azobenzenes (-N=N-) [51] and azo-coupling (-N=N-X-Y-), or from the condensation reaction of aldehyde and aniline in the case of azomethines (-CH=N-) [52]. A series of synthetically feasible stilbenes and pseudo-stilbenes was planned for this study. More details regarding the synthesis of the investigated compounds can be found in the Supplementary Information (SI).

The investigated molecules are shown in Figure 1, which are a series of pseudo-stilbenes (System I) and azobenzene-based compounds (System II) containing a donor dimethylamine group (4-NMe<sub>2</sub>) and an acceptor nitro group (4'-NO<sub>2</sub>).

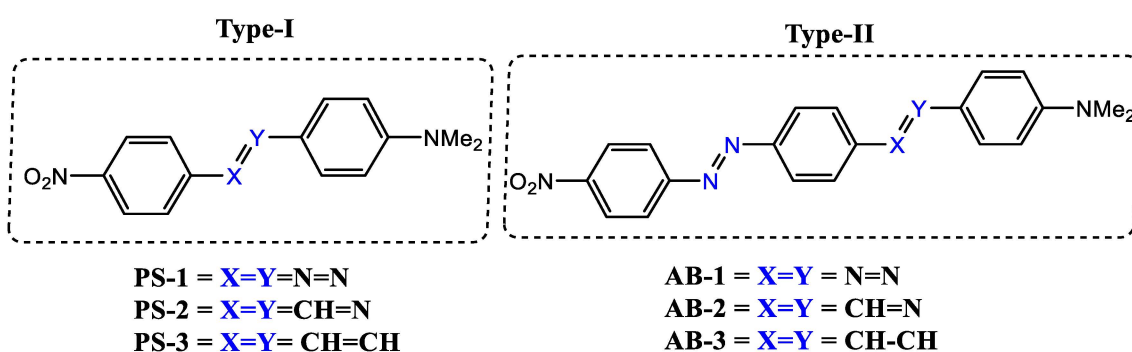


**Figure 1.** The molecular structures investigated in this work are pseudo-stilbenes (type I) and azobenzene-based compounds (type II).

## 3. Computational Methodology Details

Dynamic and static first-order hyperpolarizabilities were estimated by using QCCs performed using TD-DFT via the Gaussian 16 (rev. B.01) [53] software package. Three methods were used, i.e., the exchange-correlation functional Becke; the three-parameter, Lee–Yang–Parr (B3LYP) method [54]; and its long-range corrected version including the Coulomb-attenuating method (CAM-B3LYP) [55]. Also, a variation of a hybrid functional by Truhlar and Zhao (M06-2X) [56] optimized to predict non-covalent interactions complemented the level of theory. All functionals were combined with a triple-zeta split-valence Pople basis set [57] with two additional polarization functions for non-hydrogen atoms, one additional polarization function on hydrogen atoms, and diffuse functions on hydrogen and non-hydrogen atoms: 6-311++G(2d,p).

The computational methodology consisted of three steps: molecular structure geometry optimization, calculating the one-photon vertical excitation energies, and computing the tensor components of the first-order molecular hyperpolarizability. Then, Hyper-QCC [19], a post-processing software dedicated to computing third-order ranking tensor components in a fast and reliable way, was used for the final calculation of  $\beta_0$  and  $\beta_{HRS}$  values.

The first computational step was the geometry optimization calculation in gas-phase and solvent medium (dimethyl sulfoxide—DMSO). The solvation effect was obtained by employing a polarizable continuum model (PCM) using the integral equation formalism variant (IEF-PCM) [58]. The level of theory CAM-B3LYP was the only method used to calculate the energy minima of all compounds. The second step was to obtain the vertical excitation energies in DMSO using the same level of theory of geometry optimization. The vertical excitation energies allow us to verify the spectral transparency window of all compounds. The third step was to calculate the static ( $\omega = 0$  a.u.) and dynamic ( $\omega \neq 0$  a.u.)

tensor components, i.e.,  $\beta_{ijk}$ . As mentioned before, the frequencies used to achieve the dynamic values are equivalent to the wavelengths of 1064 nm (0.0428 a.u.), 1310 nm (0.0348 a.u.), and 1550 nm (0.0294 a.u.). All three hybrid functionals (B3LYP, CAM-B3LYP, and M06-2X) were used to obtain the hyperpolarizability tensor components in the solvent and gas phase. The Gaussian output files provided in the third step were post-processed in Hyper-QCC software v.1.3.2 to gather the final values of  $\beta_0$  and  $\beta_{HRS}$ .

The post-processing software Hyper-QCC [19] calculates the first-molecular hyperpolarizability based on the mixed spherical–cartesian formalism [59], in which the orientational averaged first-order hyperpolarizability squared  $\beta_{HRS}$  is expressed by Equation (1) [60].

$$\beta_{HRS} = \sqrt{\frac{2}{9}|\beta_{J=1}|^2 + \frac{2}{21}|\beta_{J=3}|^2} \quad (1)$$

The  $\beta_{HRS}$  tensor is decomposed as the sum of dipolar ( $J = 1$ ) and octupolar ( $J = 3$ ) tensorial components. The relationships between the dipolar and octupolar components and the cartesian components of  $\beta_{HRS}$  are described in Equations (2) and (3).

$$|\beta_{J=1}|^2 = \frac{3}{5}\sum_i \beta_{iii}^2 + \frac{6}{5}\sum_{i \neq j} \beta_{iii}\beta_{ijj} + \frac{3}{5}\sum_{i \neq j} \beta_{ijj}^2 + \frac{3}{5}\sum_{i \neq j \neq k} \beta_{ijj}\beta_{ikk} \quad (2)$$

$$|\beta_{J=3}|^2 = \frac{2}{5}\sum_i \beta_{iii}^2 - \frac{6}{5}\sum_{i \neq j} \beta_{iii}\beta_{ijj} + \frac{12}{5}\sum_{i \neq j} \beta_{ijj}^2 - \frac{3}{5}\sum_{i \neq j \neq k} \beta_{ijj}\beta_{ikk} + \sum_{i \neq j \neq k} \beta_{ijk}^2 \quad (3)$$

#### 4. Results and Discussion

Both investigated systems (type-I and -II) are push–pull systems in which the linear and nonlinear optical properties depend on the functional and peripheral groups present in each molecular structure, as well as on the increase in pi-conjugate bonds [26,61]. Thus, an understanding of the strength of the donor and acceptor substituents and the nature of the  $\pi$ -bridge is essential to discuss how ICT will affect the  $\beta_{HRS}$  values. As mentioned before, the  $\beta_{HRS}$  values of all compounds were calculated in the gas phase and medium solvent at their minimum energies. Section S1 of the SI presents all optimized cartesian coordinates. The 3D illustration in Figure 2 shows the visualization in different planes of the molecules: (a) front view, (b) planar view, and (c) side view. This visualization was generated using GaussView 6, a graphical interface used with Gaussian.

With the minimum energy obtained, we investigated planarity (geometric) parameters, such as the bond length, bond angle, and twist (torsion) angle for all compounds in solvent medium (DMSO). Planarity implies that all atoms within the molecule are arranged in the same plane, meaning that the angles between atoms are at  $180^\circ$ , with no significant deviations from the ideal planar structure. The planarity of the molecule can be experimentally evaluated through measurements like the average deviation of atoms from the plane defined by a set of reference atoms or through theoretical calculations. In the compounds investigated, central torsion angles ( $-X = Y$ -) and torsion angles near the NMe<sub>2</sub> substituent were selected to evaluate each molecule's planar structure. Planar conformations can affect the interactions of donor and acceptor groups throughout the molecule, resulting in varying electronic mobilities and optical nonlinearities. Third-party software was used to obtain parameters related to bond length (Å), bond angle (Å), and torsion angle (°). The methodology employed for these determinations is outlined as follows: (i) import the input file containing the XYZ coordinates of the optimized compound; (ii) examine the molecular structure in three dimensions to measure the distance, angles, and torsion with tools available in the software; (iii) calculate distances by selecting pairs of atoms; (iv) calculate angles by selecting three atoms that make up the angle of interest; and (v) calculate molecular torsion by selecting four adjacent atoms along the main chain and near the substituents at the end of the molecular chain. All the methodology results are presented in Table 1.

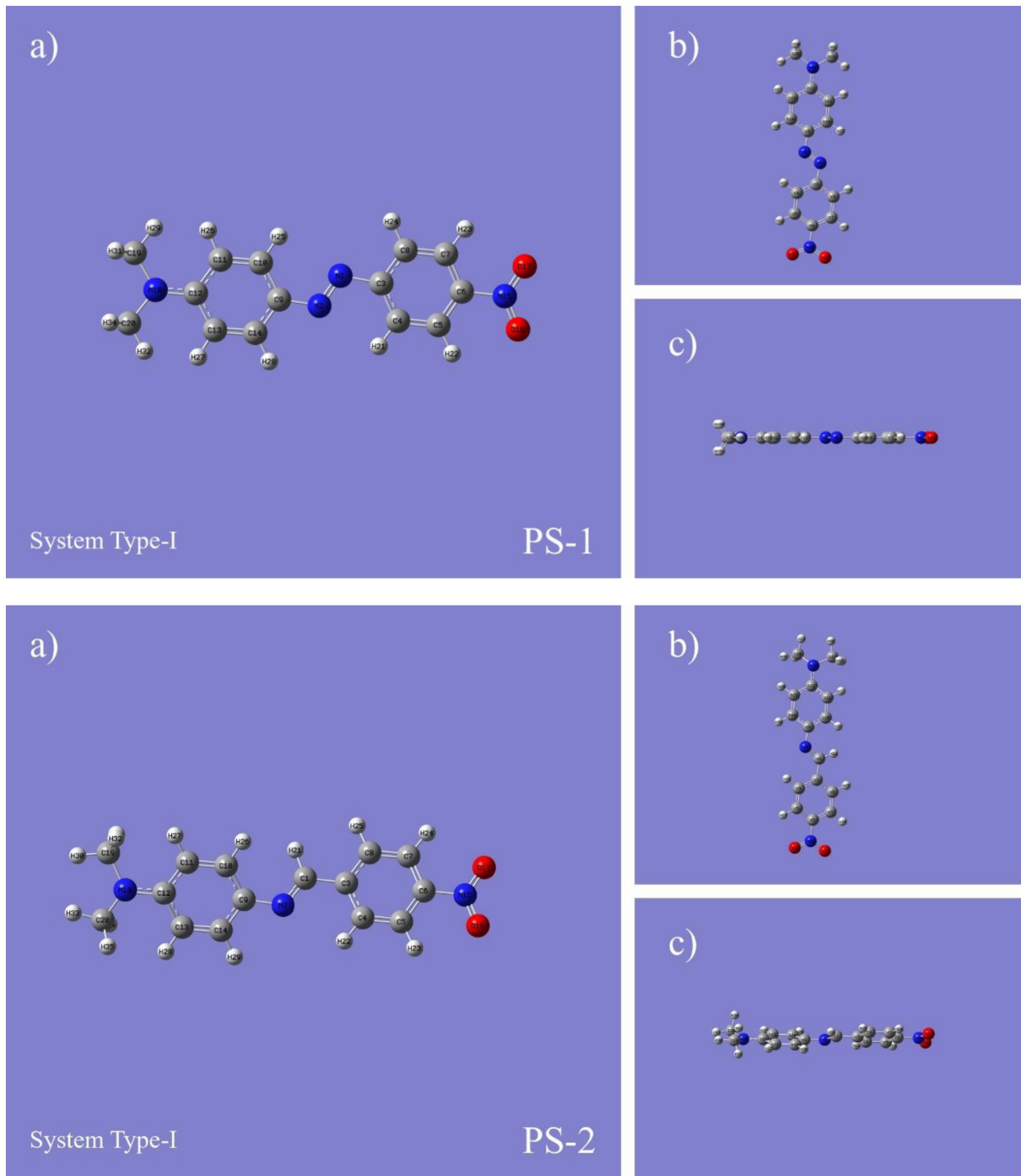
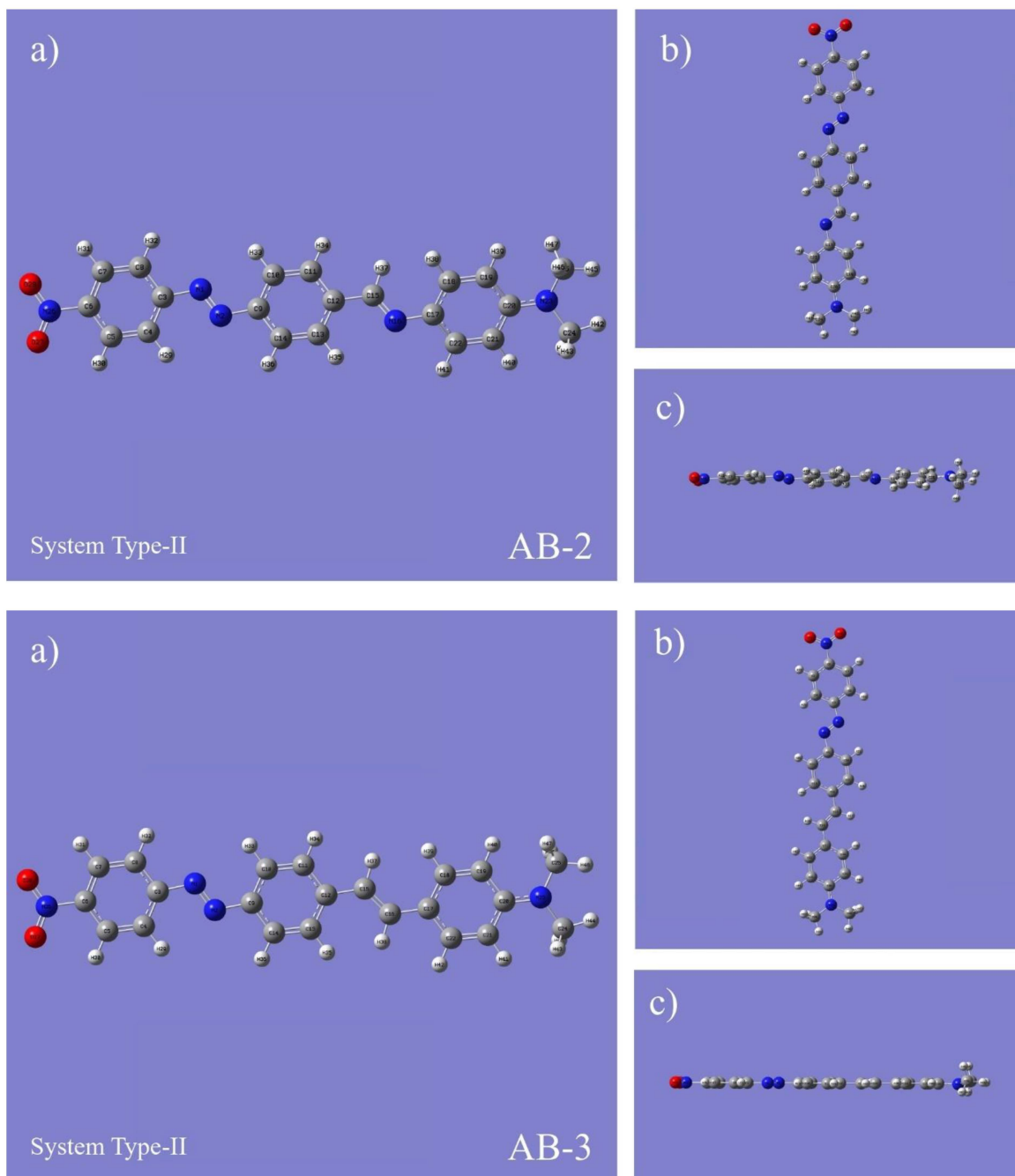


Figure 2. Cont.





**Figure 2.** Graphical representations regarding the views of all investigated molecular structures in (a) front view, (b) planar view, and (c) side view. All results were obtained after geometry optimization using the CAM-B3LYP/6-311++G(2d, p) level of theory. The colors in the illustration represent the atoms within the compounds, where carbon is depicted in gray, hydrogen in white, nitrogen in blue, and oxygen in red.

The planarity parameters were compared from the central core of the molecules to the connection between the donor and acceptor groups, aiming to analyze the main structural changes, which can be a reasonable indication of charge transfer. In all investigated systems, it is possible to observe favorable planarity; however, the molecular structures containing the azomethine group (CH=N), i.e., PS-2 and AB-2, deviate slightly from molecular planarity. This variation suggests that it is due to three main factors: increased conjugation and the interaction between the functional group and both the electron-donating (-NMe<sub>2</sub>) and -accepting (-NO<sub>2</sub>) groups. On the other hand, for compounds AB-1 and AB-3, we noticed that, despite the increase

in the  $\pi$ -conjugated chain, the planarity of the molecules was preserved. Consequently, this can directly influence the optical properties of these systems.

In this context, when examining the spectroscopic parameters listed in Table 2, it is noteworthy that compounds with elevated dipole moment values exhibited minimal deviations from their planar configuration. We analyzed each structure's main torsions and bond angles to verify this result. Initially, we observed some deviations in the torsions between the functional groups that bind the phenyls, which presented the following values: PS-1 (179.99°), PS-2 (178.07°), PS-3 (179.96°), AB-1 (179.99°), AB-2 (179.60°), and AB-3 (179.96°). From the analysis, we noticed that the PS-2 compound shows a twisting of 1.93° in relation to other planar structures (PS-1, PS-3, AB-1, and AB-3), while compound AB-2 exhibits a variation of 0.4°. Therefore, when analyzing the torsions within the plane of the functional groups -NO<sub>2</sub> and -NMe<sub>2</sub>, we observed that the greatest torsions occur towards the donor group, with the following values: PS-1 (179.98 Å), PS-2 (169.59°), PS-3 (169.67°), AB-1 (179.92°), AB-2 (−166.35°) and AB-3 (169.43°). The lowest values were for compounds AB-2, PS-2, AB-3, and PS-3, respectively. This observation is relevant, as it can influence the NLO response, given that these structural changes may lead to modifications in the dipole moment values and the first molecular hyperpolarizability [62–65]. In general, larger dipole moments tend to result in larger NLO responses. Therefore, organic compounds with larger dipole moments exhibit more robust nonlinear optical properties. However, the relationship between dipole moments and NLO responses can be affected by a variety of factors, including the molecular structure and the chemical environment [18].

**Table 1.** Bond length, bond angle, and torsion angle of all compounds investigated in this work after geometry optimization in solvent medium (DMSO).

Compounds		Bond Length (Å)		Bond Angle (Å)		Torsion Angle (°)	
System Type I	PS-1	C3-N1	1.418	C3-N1-N2	114.59	C3-N1-N2-C9	179.99
		N1-N2	1.250	N1-N2-C9	116.24	O17-N15-C6-C5	−179.99
		N2-C9	1.392	C6-N15-O17	117.57	C20-N18-C12-C11	−179.98
		C6-N15	1.461	C6-N15-O16	117.66	N2-C9-C10-C12	−179.99
		C12-N18	1.372	C12-N18-C19	124.19	N1-N2-C10-C9	−0.001
		N18-C19	1.459	C12-N18-C20	123.93	N1-N2-C3-C4	−0.001
		N18-C20	1.457	C5-C6-N15	118.95	C12-C11-C10-N18	−179.99
		N3-O1	1.217	C11-C12-N18	121.63	C6-C5-C4-N15	180.00
	N3-O2	1.217	C12-C11-C10	120.56	C5-C4-C6-N1	180.00	
	PS-2	C15-N3	1.268	C3-C1-N2	122.04	C9-N2-C1-C3	178.07
		C14-C15	1.469	C9-N2-C1	121.07	C5-C6-N15-O17	179.97
		N3-C8	1.405	C6-N15-O16	117.70	C20-N18-C12-C11	−169.59
		C5-N1	1.375	C6-N15-O17	117.72	N15-C6-C5-C4	179.95
		C11-N2	1.461	C19-N18-C12	119.05	O17-N15-C5-C4	178.79
		N1-C2	1.449	C20-N18-C12	119.05	C4-C3-C1-N2	−11.62
		N1-C16	1.450	N15-C6-C8	118.97	O16-N15-C6-C5	−0.02
		N2-O1	1.220	N18-C12-C11	121.35	N18-C12-C11-C10	178.80
	N2-O2	1.220	C12-C11-C10	121.23	C11-C10-C9-C2	179.72	
	PS-3	C1-C2	1.335	C1-C2-C3	126.27	C1-C2-C3-C9	179.96
		C1-C3	1.460	C1-C2-C9	127.36	C5-C6-N15-O17	179.90
		C2-C9	1.457	C6-N15-O16	117.80	C20-N18-C12-C11	−169.67
C12-N18		1.376	C6-N15-O17	117.82	C6-C5-C4-C3	−179.82	
N18-C19		1.446	C12-N18-C19	119.43	C1-C2-C3-C4	−0.21	
N18-C16		1.446	C12-N18-C20	119.25	C19-N18-C12-C11	11.08	
N15-C6		1.461	C11-C12-N18	121.37	C5-C6-N15-O16	−0.12	
N15-O17		1.218	C4-C3-C1	123.46	C6-C5-C4-N15	−179.91	
N15-O18	1.218	C2-C9-C10	123.95	C10-C11-C12-N18	178.46		

Table 1. Cont.

Compounds		Bond Length (Å)		Bond Angle (°)		Torsion Angle (°)	
AB-1	C3-N1	1.421	C3-N1-N2	114.75	C3-N1-N2-C9	179.99	
	N1-N2	1.240	N1-N2-C9	115.70	C6-C5-N23-O25	179.99	
	N2-C7	1.413	C12-N15-N16	114.82	C12-N15-N16-C17	−180.00	
	C9-N3	1.416	N15-N16-C17	116.09	N26-C20-C19-C18	179.08	
	N15-N16	1.244	C27-N26-C20	121.07	C28-N26-C20-C19	−173.93	
	N15-C12	1.417	C28-N26-C20	119.83	N1-N2-C9-C10	−0.04	
	N16-C13	1.402	C6-N23-O24	117.67	N15-N16-C17-C18	−0.37	
	C20-N26	1.369	C6-N23-O25	117.68	C5-C4-C3-N1	−179.99	
	N26-C27	1.447	C6-C5-N23	118.85	C11-C10-C9-N2	179.99	
	N26-C28	1.446	C22-C21-C20	120.60	N15-C12-C11-C10	179.99	
	C6-N23	1.468	C6-C5-C5	118.95	C27-N26-C20-C19	−6.73	
	N23-O24	1.216			C4-C5-C6-N23	−179.99	
N23-O25	1.216						
AB-2	C3-N1	1.421	C3-N1-N2	114.89	C3-N1-N2-C9	179.60	
	N1-N2	1.239	N1-N2-C9	115.72	C12-C15-N16-C17	−178.13	
	N2-C9	1.416	C12-C15-N16	122.52	C25-N23-C19-C20	166.35	
	C12-C15	1.467	C17-N15-C1	120.67	N23-C20-C19-C18	177.52	
	C15-N16	1.268	C20-N23-C25	119.03	C19-C18-C17-N16	179.40	
	N16-C17	1.406	C20-N23-C24	118.95	N1-N2-C9-C10	−0.72	
	C20-N23	1.378	C6-N23-O28	118.12	C18-C17-N16-C15	−29.74	
	N23-C25	1.449	C5-C6-N23	118.78	C25-N23-C20-C19	12.36	
	N23-C24	1.450	C19-C20-N23	121.51	C5-C6-N26-O27	0.20	
	C6-N26	1.463			C5-C6-N26-O28	−179.98	
	N26-O28	1.219			C11-C12-C15-N16	−178.88	
	N26-O27	1.219					
AB-3	C3-N1	1.420	C3-N1-N2	114.83	C3-N1-N2-C9	−179.96	
	N1-N2	1.242	N1-N2-C9	116.06	C12-C15-C16-C17	179.98	
	N2-C9	1.409	C12-C15-C16	126.23	C24-N23-C20-C19	−169.43	
	C12-C15	1.460	C15-C16-C17	127.24	C25-N23-C20-C19	−11.30	
	C15-C16	1.338	C24-N23-C24	119.33	N23-C20-C19-C18	−178.83	
	C16-C17	1.457	C24-N23-C25	119.50	C5-C6-N26-O27	0.03	
	C20-N23	1.373	C6-N26-O27	118.15	C5-C6-N26-O28	−179.96	
	N23-C25	1.449	C6-N26-O28	118.16	C4-C5-C6-N26	180.00	
	N23-C24	1.450	C19-C20-N23	121.41	C16-C15-C12-C11	−179.92	
	N26-C6	1.462	C5-C6-N26	118.83	C11-C10-C12-N2	−179.98	
	N26-O27	1.219	C20-C19-C18	121.28	C19-C18-C17-C16	−179.96	
	N4-O28	1.219	C4-C5-C6	118.91			

When analyzing the bond angles, we observed similar behavior in most compounds, except for PS-2. In the specific case of PS-2, we noted that the C3-C1-N2 angle, toward the phenyl that binds the NO<sub>2</sub> group, is 122.04 Å, while the C1-N3-C9 angle towards the phenyl that binds the NMe<sub>2</sub> group is 121.07 degrees, resulting in a deviation of 0.97 degrees between the angles. The other central bond angles present slightly higher values towards the plane of the NMe<sub>2</sub> group, as highlighted in the Table 1 (in bold). Furthermore, the systems exhibit deviations of 1.65 Å, 1.09 Å, 0.89 Å, 0.95 Å, and 1.23 Å, for PS-1, PS-3, AB-1, AB-2, and AB-3, respectively.

The molecular structures PS-1 and PS-2 were the only ones found deposited in the Cambridge Crystallographic Data Center (CCDC) database, which reports the single crystal X-ray analysis, recorded with crystallographic information numbers (CIF) 234915 (PS-1) and 1217889 (PS-2) (see Supplementary Materials Table S1). CCDC data allowed us to

compare our theoretical results for PS-1 and PS-2 with their experimental analogs. Such a comparison revealed a slight difference between the gas phase and the solid phase, with an emphasis on the central torsion and the torsion caused by the acceptor and donor groups, which can be justified due to the crystalline packing of these compounds, clearly evidencing a significant difference between the molecular and crystalline structure [66–68].

**Table 2.** Spectroscopic parameters regarding the lowest energy transitions retrieved from calculated excitation energies of all compounds in DMSO medium using CAM-B3LYP/6-311++G(2d,p) level of theory.  $\lambda_{max}$ , is the maximum absorption wavelength;  $f_{osc}$  is the oscillator strength;  $\mu$  (D) is the permanent dipole moment.

Compounds		$\lambda_{max}(nm)$ [eV] Transition	$f_{osc}$	$\mu$ (D)
System Type I	PS-1	442 [2.80] {S <sub>0</sub> -S <sub>1</sub> }	0.00	13.86
		436 [2.84] {S <sub>0</sub> -S <sub>2</sub> }	1.61	
	PS-2	412 [3.01] {S <sub>0</sub> -S <sub>1</sub> }	1.06	10.52
System Type II	PS-3	423 [2.93] {S <sub>0</sub> -S <sub>1</sub> }	1.56	12.56
System Type II	AB-1	462 [2.68] {S <sub>0</sub> -S <sub>1</sub> }	0.00	14.03
		455 [2.73] {S <sub>0</sub> -S <sub>2</sub> }	2.15	
	AB-2	462 [2.68] {S <sub>0</sub> -S <sub>1</sub> }	0.00	10.62
AB-3	428 [2.90] {S <sub>0</sub> -S <sub>2</sub> }	1.53		
	AB-3	460 [2.69] {S <sub>0</sub> -S <sub>1</sub> }	1.99	13.23

Understanding linear optical effects, like one-photon absorption (OPA), is crucial for determining the transparency range of the samples under investigation. Specifically, we aimed to ascertain if the sample possesses a clear transparency window at approximately 532 nm and beyond. Therefore, before evaluating  $\beta_{HRS}$ , we aimed to explore the characteristics of the vertical transitions linked to the compounds in question. Also, by using TD-DFT calculations, we determined the vertical excitation energies in the DMSO medium, presented in Table 2. It can thus be inferred that all compounds offer a distinct transparency window commencing at ca. 500 nm. This suggests that any ISHG emissions prompted by incident light at 1064 nm, or greater wavelengths, would not be reabsorbed within the medium. Figure 3 illustrates all the vertical transitions associated with OPA simulations using the CAM-B3LYP/6-311++G(2d,p) level of theory. Moreover, a zero or very low probability of vertical transitions around 532 nm will also reduce the probability of two-photon absorption transitions, which could influence the  $\beta_{HRS}$  results, as reported by L. Sciuti et al. [69].

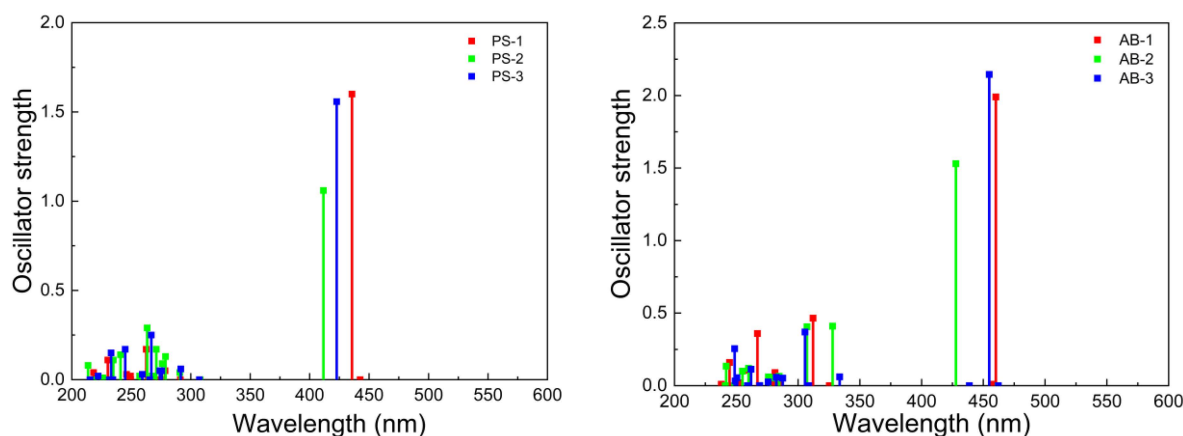


**Figure 3.** TD-DFT calculations were used to obtain the vertical transitions for system type I and II molecules using the CAM-B3LYP/6-311++G(2d,p) level of theory in solvent medium (DMSO).

The permanent dipole moment ( $\mu$ ) value, also calculated via TD-DFT, can be used, for example, to compare the values of the investigated compounds with reference SHG compounds, such as paranitroaniline (PNA), urea, and potassium dideuterium phosphate (KDP). All investigated compounds presented dipole moments ranging from 10.52 D to 14.03 D, which are greater than the ones calculated for PNA (7.86 D), urea (5.91 D), and KDP (10.28 D) in solvent medium. Among the investigated molecular structures, the lowest  $\mu$  values belong to PS-2 (~10.5 D) and AB-2 (~10.6 D), while the highest ones belong to PS-1 (~13.9 D) and AB-2 (~14.0 D). Since the peripheral groups are the same on both molecules, the azomethine functional group (CH=N) present in PS-2 and AB-2 reduces the  $\mu$  value. On the other hand, PS-1 and AB-2, with an azo functional group (N=N), have higher  $\mu$  values. PS-3 and AB-3, with a vinyl functional group (CH=CH), have intermediate  $\mu$  values in this work, with ~12.6 D and ~13.2 D, respectively. The calculated  $\mu$  values are consistent with the ones reported in the literature [34,49].

Finally, all calculated  $\beta_0$  and  $\beta_{HRS}$  values are presented in Supplementary Materials Tables S3-A–S3-I in the SI for the investigated and reference compounds, PNA, urea, and KDP, under the same computational conditions. The highest  $\beta_{HRS}$  values were obtained using the B3LYP level of theory; this level of theory is well known to overestimate first-order hyperpolarizability calculations [15,70]. HRS is not a resonant process, but the contribution of the permanent and transition dipole moments could strongly influence  $\beta_{HRS}$ , according to the semi-classical time-dependent perturbation theory proposed by Orr and Ward [71]. According to Orr and Ward, if the transition dipole moment between the ground and the first excited state ( $\mu_{01}$ ) exhibits a higher value and aligns more closely with the incident frequency ( $\lambda_{\mu_{01}} \rightarrow \lambda_{HRS}$ ), this proximity indicates a scenario nearing resonance absorption. In such cases, it is expected that both  $\beta_0$  and  $\beta_{HRS}$  will exhibit greater values compared to situations with lower  $\mu_{01}$  and  $\lambda_{\mu_{01}}$ . Therefore, this can justify  $\beta_0$  and  $\beta_{HRS}$  overestimations because B3LYP usually enhances oscillator forces and results in a bathochromic shift in their spectral position compared with the experimental values of one-photon absorption of organic compounds [47,72].

Choosing the most suitable level of theory to predict the true value of  $\beta_{HRS}$  is not easy, especially when no experimental results are reported. However, CAM-B3LYP and M06-2X are probably the most suitable levels of theory to estimate the linear and nonlinear optical responses of these types of organic compounds, as previously reported and compared with experimental values [34,40,48,72–74]. Moreover, as mentioned in the introduction section, Krawczyk, P. [49] has calculated  $\beta_0$  values for compounds PS-1, -2, and -3, which corroborate the observation of the tendency for overestimated values of the first-molecular hyperpolarizability when using B3LYP, as shown in Table 3. The  $\beta_0$  values calculated by Krawczyk, P. show some variation compared to our results, which could be explained by the different approaches, i.e., Møller–Plesset perturbation (MP2), HF methods, BLYP, B3LYP, and the CAM-B3LYP functionals, used to calculate  $\beta_0$ , as well as the different software QCC package (GAMESS 2023 R2 and Dalton 2.0). For all investigated compounds in our work, both  $\beta_0$  and  $\beta_{HRS}$  values are indeed overestimated when calculated with B3LYP.

In the photonics field context, particularly in optical communications, the most important results are associated with  $\beta_{HRS}$ . Therefore, we direct the reader to our estimated  $\beta_{HRS}$  results exclusively obtained with CAM-B3LYP and M06-2X, which returned similar values. The M06-2X level of theory, as far as we know, was first used to compute first-order molecular hyperpolarizabilities by Castet et al. [13]. Figure 4 depicts  $\beta_{HRS}$  values with CAM-B3LYP/6-311+G(2d,p) used at three distinct incident wavelengths, including the two most used wavelengths, so far, in optical communications (1310 nm and 1550 nm).

**Table 3.** Calculated values of static first-order molecular hyperpolarizability of all compounds using the B3LYP and CAM-B3LYP level of theory using the 6-311++G(2d, 2p) basis set with an incident wavelength of 1064 nm. All values are presented in units of  $10^{-30} \text{ cm}^4 \text{ statvolt}^{-1}$  both in the gas phase and solvent medium.

Level of Theory	$\beta_0$ in a Vacuum			$\beta_0$ in DMSO		
	PS-1	PS-2	PS-3	PS-1	PS-2	PS-3
B3LYP	73.2 <sup>a</sup> (144.30) <sup>b</sup>	103.4 <sup>a</sup> (165.0) <sup>b</sup>	95.9 <sup>a</sup> (152.1) <sup>b</sup>	356.0 <sup>a</sup> (626.4) <sup>a</sup>	434.6 <sup>a</sup> (938.5) <sup>b</sup>	463.7 <sup>a</sup> (927.6) <sup>b</sup>
CAM-B3LYP	50.0 <sup>a</sup> (74.6) <sup>b</sup>	42.5 <sup>a</sup> (74.7) <sup>b</sup>	50.5 (86.5) <sup>b</sup>	181.5 <sup>a</sup> (113.2) <sup>b</sup>	127.6 <sup>a</sup> (112.4) <sup>b</sup>	187.4 <sup>a</sup> (123.4) <sup>b</sup>

The values were converted from atomic units to electrostatic unities using  $1 \text{ a.u.} = 8.641 \times 10^{-33} \text{ esu}$ . <sup>a</sup> this work, using the Gaussian 16 (rev. B.01) software package; <sup>b</sup> values in parentheses were taken from ref. [49] using GAMESS and Dalton 2.0 with the 6-311++G(d,p) basis set.

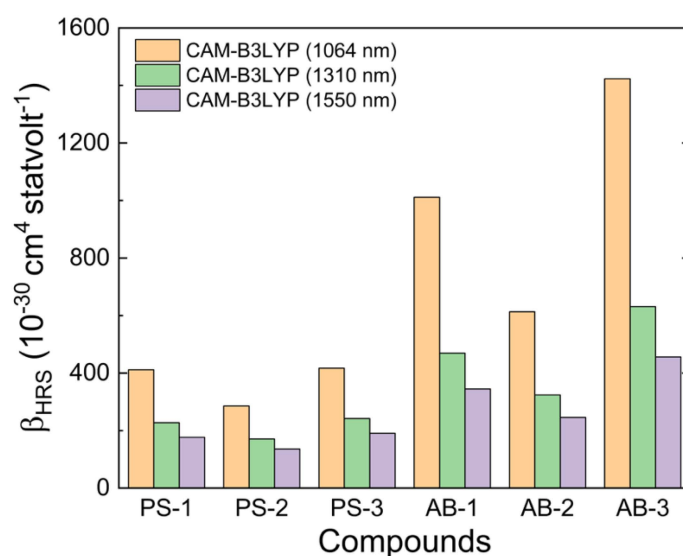


**Figure 4.** Calculated dynamic first-order molecular hyperpolarizability  $\beta_{HRS}$  of the investigated compounds in solvent medium (DMSO) at three incident wavelengths (1064 nm, 1310 nm, and 1550 nm) using CAM-B3LYP/6-311++G(2d,p).

One can see that the compounds belonging to system type-2 (AB-1, -2, and -3) presented higher values than their analogs from system type-1 (PS-1, -2, and -3), regardless of the incident wavelength. For example, the highest  $\beta_{HRS}$  magnitude difference is between AB-3 and PS-3, in which  $\beta_{HRS}$  has tripled ( $\beta_{HRS_{AB-3}}^{1064 \text{ nm}} \sim 1424$  vs.  $\beta_{HRS_{PS-3}}^{1064 \text{ nm}} \sim 417$ ). The same magnitude behavior was found from AB-1 to PS-1 ( $\beta_{HRS_{AB-1}}^{1064 \text{ nm}} \sim 1011$  vs.  $\beta_{HRS_{PS-3}}^{1064 \text{ nm}} \sim 412$ ). On the other hand, the smallest difference, but still double in value, was found from AB-2 to PS-2 ( $\beta_{HRS_{AB-2}}^{1064 \text{ nm}} \sim 613$  vs.  $\beta_{HRS_{PS-2}}^{1064 \text{ nm}} \sim 286$ ). Regarding the most suitable incident wavelengths for optical communications (1310 nm and 1550 nm), we observe the same tendency, i.e., the higher values belong to AB-3, however, with lower  $\beta_{HRS}$  magnitudes ( $\beta_{HRS_{AB-3}}^{1310 \text{ nm}} \sim 631$  and  $\beta_{HRS_{AB-3}}^{1550 \text{ nm}} \sim 456$ ).

However, it is essential to note that the reported values are still significantly higher than PNA, urea, and KDP. As mentioned before, these are compounds used as references in many experimental works [10,75–78] at least at an incident light of 1064 nm. Thus, we used PNA, urea, and KDP to establish a reliable benchmark, allowing us to draw significant conclusions about the NLO activity of the materials under investigation. For example, we obtained values of  $0.2 \times 10^{-30} \text{ esu}$ ,  $0.5 \times 10^{-30} \text{ esu}$ , and  $21.5 \times 10^{-30} \text{ esu}$  for KDP, urea, and PNA, which are in good agreement with previous reports found in the literature. Nevertheless, the values obtained for the pseudo-stilbenes and azobenzenes

investigated here are up to sixty-five, thirty-seven, and thirty times higher than PNA and hundreds of times greater than urea and KDP at the wavelengths of 1064 nm, 1330 nm, and 1550 nm, respectively. The results were compared under the same conditions of solvent medium (DMSO) and level of theory. The difference in the  $\beta_{HRS}$  magnitude between the investigated compounds and the reference ones reflects the increased  $\pi$ -conjugation and molecular size in pseudo-stilbene and azobenzene compared to the reference compounds. The observed differences in  $\beta_{HRS}$  values reflect the underlying fundamental principles of molecular structure and electronic distribution, affirming the validity and relevance of the investigated compounds as OFCs.

Additionally, it was found that the  $\beta_{HRS}$  of the compounds studied is strongly influenced by the central torsion angle and the torsion angle close to the -NMe<sub>2</sub> substituent group, and is potentially improved by the presence of CH=CH and N=N functional groups and increased conjugation, as indicated in Table 4. Furthermore, it is observed that the largest torsion angles were noted for the compounds PS-2 and AB-2, corroborating the lowest values of dipole moment and first-order molecular hyperpolarizability, respectively. However, compound AB-3, despite having good planarity and the highest first hyperpolarizability value, exhibits a decrease in the dipole moment value. This suggests that the twist near the -NMe<sub>2</sub> group may have had a significant influence.

**Table 4.** Relationship between geometric and optical parameters for all molecules using CAM-B3LYP/6-311+G(2d,p) level of theory.

Compounds		Center (-X=Y-) Torsion Angle (°)	NMe <sub>2</sub> Torsion Angle (°)	$\mu$ (D)	$\beta_{HRS}$
System Type I	PS-1	179.99	179.98	13.86	411.6
	PS-2	178.07	169.59	10.52	285.5
	PS-3	179.96	169.67	12.56	417.0
System Type II	AB-1	179.99	179.08	14.03	1011.3
	AB-2	179.60	166.35	10.62	613.1
	AB-3	179.96	169.43	13.23	1423.5

The properties of NLO depend on several structural factors, such as molecular planarity, charge transfer between side groups, conjugation length, chemical environment, and the effect of intermolecular interactions [27]. Compound AB-2 (system type-I) shows an increased conjugation length with intermolecular interactions C-H  $\cdots$   $\pi$ . However, it presents a non-planar conformation with a twisted structure, significantly reducing  $\mu$  and  $\beta_{HRS}$  values compared to the other molecules of system II. In addition, structural modifications to system type-II seem to improve the optical activity compared to system type-I, revealing the higher potential of this system for OFC applications.

## 5. Conclusions

This comprehensive investigation into the linear and nonlinear optical properties of two novel organic molecular systems (type-I and type-II) provides valuable insight into the intricacies of push-pull systems, mainly how they affect the  $\beta_{HRS}$  magnitude. The correlation between molecular structure and  $\beta_{HRS}$  response was evident, particularly the significance of the azomethine group (CH=N) in affecting the planarity and optical properties. The presence of this group led to reduced molecular planarity in some compounds, which in turn influenced the overall  $\beta_{HRS}$  response. Predicted  $\beta_{HRS}$  values, which are particularly important for photonics and optical communications applications, were significantly more significant for the type-II system (AB-1, -2, and -3) than their type-I counterparts (PS-1, -2, and -3). Especially when considering optical communication wavelengths of 1310 nm and 1550 nm, the type-II system consistently outperformed the type-I system. The compounds studied in this work exhibited  $\beta_{HRS}$  values that substantially surpassed those

of reference compounds PNA, urea, and KDP. This comparative analysis emphasized the potential of these molecules for applications requiring robust NLO properties. Moreover, it shows that the novel molecular design (type-II) presented in this work has the potential to be used for photonic crystals with the ability for nonlinear optical conversion.

However, there are significant challenges to predicting  $\beta_{HRS}$ , such as the overestimation and underestimation of  $\beta_{HRS}$  when utilizing different levels of theory. For example, using the functional B3LYP level of theory led to an overestimation of the magnitude compared with the other two functionals (CAM-B3LYP and M06-2X). Choosing an accurate level of theory to predict the true value of  $\beta_{HRS}$  proved complex, especially when no experimental data were available for comparison. As far as we know, there is no reported work with experimental  $\beta_{HRS}$  values measured via the HRS or EFISH techniques. Therefore, the comparison between experimental and theoretical  $\beta_{HRS}$  was not possible. In this case, the absence of experimental results will not be thought of as a drawback of our work. On the contrary, it confirms the novelty of this current work. Moreover, such novelty could encourage chemical research groups to synthesize compounds of system type-II for future experiments, which will verify the true potential of these organic compounds in OFC devices. Organic OFCs with high responses have the potential to revolutionize communication and data transmission due to their potential to offer incredibly high speeds, greater bandwidths, and lower signal losses.

**Supplementary Materials:** The following supporting information can be downloaded at: <https://www.mdpi.com/article/10.3390/photonics11030283/s1>, Optimized Geometries, 1.; Geometric parameters of the compounds, 2.; First-Order Molecular Hyperpolarizability Calculation, 3.; Methods of Synthesis for the Investigated Compounds, 4.

**Author Contributions:** Conceptualization, L.M.G.A.; methodology, L.M.G.A.; validation, L.M.G.A., J.J.R.J. and M.A.R.C.A.; formal analysis, R.S.A. and L.M.G.A.; investigation, R.S.A.; resources, L.M.G.A.; data curation, R.S.A.; writing—original draft preparation, L.M.G.A., J.R. and R.S.A.; writing—review and editing, J.J.R.J., M.A.R.C.A., S.S. and L.M.G.A.; visualization, R.S.A.; supervision, L.M.G.A.; project administration, L.M.G.A.; funding acquisition, J.J.R.J. and L.M.G.A. All authors have read and agreed to the published version of the manuscript.

**Funding:** This research was funded by Conselho Nacional de Desenvolvimento Científico e Tecnológico (CNPq), with the following grant numbers 151202/2023-0, 311439/2021-7, 406190/2021-6 and 440225/2021-3; Fundação de Amparo à Pesquisa do Estado de Goiás (FUNAPE), grant number 1/2022; and Fundação de Amparo à Pesquisa do Estado de São Paulo (FAPESP), grant number 2023/11153-4; National Institute of Photonics (INCT de Fotônica), grant number 465763/2014-6, MCTI/CNPq/FACEPE.

**Institutional Review Board Statement:** Not applicable.

**Informed Consent Statement:** Not applicable.

**Data Availability Statement:** The data presented in this study are available on request from the corresponding author.

**Acknowledgments:** Coordenação de Aperfeiçoamento de Pessoal de Nível Superior (CAPES)—Brasil; FAPITEC/SE (Fundação de Apoio à Pesquisa à Inovação Tecnológica do Estado de Sergipe). Finally, this research was supported by LaMCAD (Laboratório Multiusuário de Computação de Alto Desempenho) from Universidade Federal de Goiás.

**Conflicts of Interest:** The authors declare no conflicts of interest.

## References

1. Agrell, E.; Karlsson, M.; Chraplyvy, A.R.; Richardson, D.J.; Krummrich, P.M.; Winzer, P.; Roberts, K.; Fischer, J.K.; Savory, S.J.; Eggleton, B.J. Roadmap of optical communications. *J. Opt.* **2016**, *18*, 63002. [[CrossRef](#)]
2. Karothu, D.P.; Dushaq, G.; Ahmed, E.; Catalano, L.; Polavaram, S.; Ferreira, R.; Li, L.; Mohamed, S.; Rasras, M.; Naumov, P. Mechanically robust amino acid crystals as fiber-optic transducers and wide bandpass filters for optical communication in the near-infrared. *Nat. Commun.* **2021**, *12*, 1326. [[CrossRef](#)]

3. Feldmann, A.; Gasser, O.; Lichtblau, F.; Pujol, E.; Poese, I.; Dietzel, C.; Wagner, D.; Wichtlhuber, M.; Tapiador, J.; Vallina-Rodriguez, N. A year in lockdown: How the waves of COVID-19 impact internet traffic. *Commun. ACM* **2021**, *64*, 101–108. [[CrossRef](#)]
4. Castet, F.; Bogdan, E.; Plaquet, A.; Ducasse, L.; Champagne, B.; Rodriguez, V. Reference molecules for nonlinear optics: A joint experimental and theoretical investigation. *J. Chem. Phys.* **2012**, *136*, 24506. [[CrossRef](#)] [[PubMed](#)]
5. Franken, P.A.; Hill, A.E.; Peters, C.W.; Weinreich, G. Generation of Optical Harmonics. *Phys. Rev. Lett.* **1961**, *7*, 118–119. [[CrossRef](#)]
6. Chemla, D.S. *Nonlinear Optical Properties of Organic Molecules and Crystals*; Elsevier: Amsterdam, The Netherlands, 2012.
7. Radhakrishnan, T.P. Molecular structure, symmetry, and shape as design elements in the fabrication of molecular crystals for second harmonic generation and the role of molecules-in-materials. *Acc. Chem. Res.* **2008**, *41*, 367–376. [[CrossRef](#)] [[PubMed](#)]
8. Abegão, L.M.G.; Fonseca, R.D.; Santos, F.A.; Rodrigues, J.J.; Kamada, K.; Mendonça, C.R.; Piguel, S.; De Boni, L. First molecular electronic hyperpolarizability of series of  $\pi$ -conjugated oxazole dyes in solution: An experimental and theoretical study. *RSC Adv.* **2019**, *9*, 26476–26482. [[CrossRef](#)] [[PubMed](#)]
9. Zhao, T.; Wang, C.; Hu, S.; Ji, S.; Hu, C.; Xu, K.; Teng, B. Structural design and characterization of a chalcone derivative crystal DAMO with strong SHG efficiency for NLO applications. *Opt. Mater.* **2021**, *112*, 110765. [[CrossRef](#)]
10. De Araújo, R.S.; de Alcântara, A.M.; Abegão, L.M.G.; de Souza, Y.P.; Silva, A.C.B.; Machado, R.; Rodrigues, J.J.; Pliego, J.R.; d’Errico, F.; Valle, M.S.; et al. Second harmonic generation in pyrazoline derivatives of dibenzylideneacetones and chalcone: A combined experimental and theoretical approach. *J. Photochem. Photobiol. A Chem.* **2020**, *388*, 112147. [[CrossRef](#)]
11. López, S.F.; Meza, M.P.; Hoyos, F.T. Study of the nonlinear optical properties of 4-nitroaniline type compounds by density functional theory calculations: Towards new NLO materials. *Comput. Theor. Chem.* **2018**, *1133*, 25–32. [[CrossRef](#)]
12. Eggleton, B.J.; Vo, T.D.; Pant, R.; Schr, J.; Pelusi, M.D.; Choi, D.Y.; Madden, S.J.; Luther-Davies, B. Photonic chip based ultrafast optical processing based on high nonlinearity dispersion engineered chalcogenide waveguides. *Laser Photon. Rev.* **2012**, *6*, 97–114. [[CrossRef](#)]
13. Castet, F.; Rodriguez, V.; Pozzo, J.-L.; Ducasse, L.; Plaquet, A.; Champagne, B. Design and characterization of molecular nonlinear optical switches. *Acc. Chem. Res.* **2013**, *46*, 2656–2665. [[CrossRef](#)]
14. Wu, J.; Luo, J.; Jen, A.K.-Y. High-performance organic second- and third-order nonlinear optical materials for ultrafast information processing. *J. Mater. Chem. C.* **2020**, *8*, 15009–15026. [[CrossRef](#)]
15. Santos, F.A.; Abegão, L.M.G.; Fonseca, R.D.; Alcântara, A.M.; Mendonça, C.R.; Alencar, M.A.R.C.; Valle, M.S.; Kamada, K.; De Boni, L.; Rodrigues, J.J. Nonlinear Optical Study in a Set of Dibenzylideneacetone Derivatives with Potential for Optical Frequency Conversion. *Photonics* **2020**, *7*, 8. [[CrossRef](#)]
16. Pelosi, A.G.; Cocca, L.H.Z.; Abegão, L.M.G.; Sciuti, L.F.; Piguel, S.; De Boni, L.; Mendonça, C.R. Influence of electron-withdrawing groups in two-photon absorption of imidazopyridines derivatives. *Dyes Pigments* **2022**, *198*, 109972. [[CrossRef](#)]
17. Ekbote, A.; Patil, P.S.; Maidur, S.R.; Chia, T.S.; Quah, C.K. Structure and nonlinear optical properties of (E)-1-(4-aminophenyl)-3-(3-chlorophenyl) prop-2-en-1-one: A promising new D- $\pi$ -A- $\pi$ -D type chalcone derivative crystal for nonlinear optical devices. *J. Mol. Struct.* **2017**, *1129*, 239–247. [[CrossRef](#)]
18. Li, M.; Li, Y.; Zhang, H.; Wang, S.; Ao, Y.; Cui, Z. Molecular engineering of organic chromophores and polymers for enhanced bulk second-order optical nonlinearity. *J. Mater. Chem. C.* **2017**, *5*, 4111–4122. [[CrossRef](#)]
19. Santos, F.A.; Cardoso, C.E.R.; Rodrigues, J.J., Jr.; De Boni, L.; Abegão, L.M.G. Nonlinear Optical Materials: Predicting the First-Order Molecular Hyperpolarizability of Organic Molecular Structures. *Photonics* **2023**, *10*, 545. [[CrossRef](#)]
20. El Ouazzani, H.; Iliopoulos, K.; Pranaitis, M.; Krupka, O.; Smokal, V.; Kolendo, A.; Sahraoui, B. Second- and third-order nonlinearities of novel push–pull azobenzene polymers. *J. Phys. Chem. B.* **2011**, *115*, 1944–1949. [[CrossRef](#)]
21. Szukalski, A.; Sahraoui, B.; Kulyk, B.; Lazar, C.A.; Manea, A.M.; Mysliwiec, J. Chemical structure versus second-order nonlinear optical response of the push–pull type pyrazoline-based chromophores. *RSC Adv.* **2017**, *7*, 9941–9947. [[CrossRef](#)]
22. Wu, J.; Wilson, B.A.; Smith, D.W., Jr.; Nielsen, S.O. Towards an understanding of structure–nonlinearity relationships in triarylamine-based push–pull electro-optic chromophores: The influence of substituent and molecular conformation on molecular hyperpolarizabilities. *J. Mater. Chem. C.* **2014**, *2*, 2591–2599. [[CrossRef](#)]
23. Misra, R.; Bhattacharyya, S.P. *Intramolecular Charge Transfer: Theory and Applications*; John Wiley & Sons: Hoboken, NJ, USA, 2018.
24. Teo, K.Y.; Tiong, M.H.; Wee, H.Y.; Jasin, N.; Liu, Z.-Q.; Shiu, M.Y.; Tang, J.Y.; Tsai, J.-K.; Rahamathullah, R.; Khairul, W.M. The influence of the push–pull effect and a  $\pi$ -conjugated system in conversion efficiency of bis-chalcone compounds in a dye sensitized solar cell. *J. Mol. Struct.* **2017**, *1143*, 42–48. [[CrossRef](#)]
25. Lee, S.; Jen, M.; Jang, T.; Lee, G.; Pang, Y. Twisted intramolecular charge transfer of nitroaromatic push–pull chromophores. *Sci. Rep.* **2022**, *12*, 6557. [[CrossRef](#)] [[PubMed](#)]
26. Jaunet-lahary, T.; Chantzis, A.; Chen, K.J.; Laurent, A.D.; Jacquemin, D. Designing Efficient Azobenzene and Azothiophene Nonlinear Optical Photochromes. *J. Phys. Chem. C* **2014**, *118*, 28831–28841. [[CrossRef](#)]
27. Jasmine, G.F.; Amalanathan, M.; Roy, S.D.D. Molecular structure and charge transfer contributions to nonlinear optical property of 2-Methyl-4-nitroaniline: A DFT study. *J. Mol. Struct.* **2016**, *1112*, 63–70. [[CrossRef](#)]
28. Muniz-Miranda, F.; Pedone, A.; Muniz-Miranda, M. Spectroscopic and DFT investigation on the photo-chemical properties of a push–pull chromophore: 4-Dimethylamino-4’-nitrostilbene. *Spectrochim. Acta Part A Mol. Biomol. Spectrosc.* **2018**, *190*, 33–39. [[CrossRef](#)]
29. Sanyal, S.; Sissa, C.; Terenziani, F.; Pati, S.K.; Painelli, A. Superlinear amplification of the first hyperpolarizability of linear aggregates of DANS molecules. *Phys. Chem. Chem. Phys.* **2017**, *19*, 24979–24984. [[CrossRef](#)]

30. Shen, T.; Wang, X.-N.; Lou, H.-X. Natural stilbenes: An overview. *Nat. Prod. Rep.* **2009**, *26*, 916–935. [[CrossRef](#)]
31. Teka, T.; Zhang, L.; Ge, X.; Li, Y.; Han, L.; Yan, X. Stilbenes: Source plants, chemistry, biosynthesis, pharmacology, application and problems related to their clinical Application-A comprehensive review. *Phytochemistry* **2022**, *197*, 113128. [[CrossRef](#)]
32. Likhtenshtein, G. *Stilbenes: Applications in Chemistry, Life Sciences and Materials Science*; Wiley-VCH Verlag GmbH & Co. KGaA: Weinheim, Germany, 2009.
33. Barrett, C.J.; Mamiya, J.; Yager, K.G.; Ikeda, T. Photo-mechanical effects in azobenzene-containing soft materials. *Soft Matter* **2007**, *3*, 1249–1261. [[CrossRef](#)]
34. Day, P.N.; Nguyen, K.A.; Pachter, R. TDDFT Study of One-and Two-Photon Absorption Properties: Donor– $\pi$ – Acceptor Chromophores. *J. Phys. Chem. B* **2005**, *109*, 1803–1814. [[CrossRef](#)] [[PubMed](#)]
35. Cariati, E.; Forni, A.; Biella, S.; Metrangolo, P.; Meyer, F.; Resnati, G.; Righetto, S.; Tordin, E.; Ugo, R. Tuning second-order NLO responses through halogen bonding. *Chem. Commun.* **2007**, 2590–2592. [[CrossRef](#)] [[PubMed](#)]
36. Iftime, M.-M.; Cozan, V.; Airinei, A.; Varganici, C.; Ailiesei, G.; Timpu, D.; Sava, I. Asymmetric azomethine amines with azobenzene moieties—liquid crystalline and optical properties. *Liq. Cryst.* **2019**, *46*, 1584–1594. [[CrossRef](#)]
37. Stoilova, A.; Georgiev, A.; Nedelchev, L.; Nazarova, D.; Dimov, D. Structure-property relationship and photoinduced birefringence of the azo and azo-azomethine dyes thin films in PMMA matrix. *Opt. Mater.* **2019**, *87*, 16–23. [[CrossRef](#)]
38. De Boni, L.; Rodrigues, J.J., Jr.; dos Santos, D.S., Jr.; Silva, C.; Balogh, D.T.; Oliveira, O.N., Jr.; Zilio, S.C.; Misoguti, L.; Mendonca, C.R. Two-photon absorption in azoaromatic compounds. *Chem. Phys. Lett.* **2002**, *361*, 209–213. [[CrossRef](#)]
39. Dudek, M.; Tarnowicz-Staniak, N.; Deiana, M.; Pokładek, Z.; Samoć, M.; Matczyszyn, K. Two-photon absorption and two-photon-induced isomerization of azobenzene compounds. *RSC Adv.* **2020**, *10*, 40489–40507. [[CrossRef](#)]
40. Shalin, N.I.; Fominykh, O.D.; Balakina, M.Y. Effect of acceptor moieties on static and dynamic first hyperpolarizability of azobenzene chromophores. *Chem. Phys. Lett.* **2019**, *717*, 21–28. [[CrossRef](#)]
41. De Boni, L.; Misoguti, L.; Zilio, S.C.; Mendonça, C.R. Degenerate two-photon absorption spectra in azoaromatic compounds. *ChemPhysChem* **2005**, *6*, 1121–1125. [[CrossRef](#)]
42. Tonnelé, C.; Champagne, B.; Muccioli, L.; Castet, F. Nonlinear optical contrast in azobenzene-based self-assembled monolayers. *Chem. Mater.* **2019**, *31*, 6759–6769. [[CrossRef](#)]
43. Qian, Y.; Wang, G.; Xiao, G.; Lin, B.; Cui, Y. The first-order molecular hyperpolarizability and thermal stability of charge-transfer azo diol and azo aldimine. *Dyes Pigments* **2007**, *75*, 460–465. [[CrossRef](#)]
44. Guo, K.; Hao, J.; Zhang, T.; Zu, F.; Zhai, J.; Qiu, L.; Zhen, Z.; Liu, X.; Shen, Y. The synthesis and properties of novel diazo chromophores based on thiophene conjugating spacers and tricyanofuran acceptors. *Dyes Pigments* **2008**, *77*, 657–664. [[CrossRef](#)]
45. Andrade, A.A.; Yamaki, S.B.; Misoguti, L.; Zilio, S.C.; Atvars, T.D.Z.; Oliveira, O.N., Jr.; Mendonça, C.R. Two-photon absorption in diazobenzene compounds. *Opt. Mater.* **2004**, *27*, 441–444. [[CrossRef](#)]
46. Vivas, M.G.; Silva, D.L.; De Boni, L.; Bretonniere, Y.; Andraud, C.; Laibe-Darbour, F.; Mulatier, J.-C.; Zales, R.; Bartkowiak, W.; Canuto, S. Experimental and theoretical study on the one-and two-photon absorption properties of novel organic molecules based on phenylacetylene and azoaromatic moieties. *J. Phys. Chem. B* **2012**, *116*, 14677–14688. [[CrossRef](#)]
47. Day, P.N.; Pachter, R.; Nguyen, K.A. Analysis of nonlinear optical properties in donor–acceptor materials. *J. Chem. Phys.* **2014**, *140*, 184308. [[CrossRef](#)]
48. Ohta, K.; Antonov, L.; Yamada, S.; Kamada, K. Theoretical study of the two-photon absorption properties of several asymmetrically substituted stilbenoid molecules. *J. Chem. Phys.* **2007**, *127*, 84504. [[CrossRef](#)] [[PubMed](#)]
49. Krawczyk, P. DFT study of linear and nonlinear optical properties of donor-acceptor substituted stilbenes, azobenzenes and benzilideneanilines. *J. Mol. Model.* **2010**, *16*, 659–668. [[CrossRef](#)]
50. Doraghi, F.; Yousefnejad, F.; Farzipour, S.; Aledavoud, S.P.; Larijani, B.; Mahdavi, M. Recent advances in synthesis of stilbene derivatives via cross-coupling reaction. *Org. Biomol. Chem.* **2023**, *21*, 1846–1861. [[CrossRef](#)]
51. Zhang, Z.-H.; Peng, S.-Q.; Chi, S.; Chen, H.; Fan, L.; Liu, Y.; Ma, X.; Huang, M.-H. Isolated-alkene-linked porous organic polymers (BIT-POPs): Facile synthesis via ROMP and distinguishing overlapping signals in solid-state <sup>13</sup>C NMR. *Polym. Chem.* **2021**, *12*, 6745–6754. [[CrossRef](#)]
52. Jorge, J.; Santos, K.F.D.P.; Timóteo, F.; Vasconcelos, R.R.P.; Cáceres, O.I.A.; Granja, I.J.A.; de Souza, J.; Monteiro, D.; Frizon, T.E.A.; Botteselle, G.D.V. Recent Advances on the Antimicrobial Activities of Schiff Bases and their Metal Complexes: An Updated Overview. *Curr. Med. Chem.* **2024**. [[CrossRef](#)]
53. Frisch, M.J.; Trucks, G.W.; Schlegel, H.B.; Scuseria, G.E.; Robb, M.A.; Cheeseman, J.R.; Scalmani, G.; Barone, V.; Petersson, G.A.; Nakatsuji, H.; et al. *Gaussian 16, Rev. C.01*; Gaussian, Inc.: Wallingford, CT, USA, 2016.
54. Lee, C.; Yang, W.; Parr, R.G. Development of the Colle-Salvetti correlation-energy formula into a functional of the electron density. *Phys. Rev. B* **1988**, *37*, 785. [[CrossRef](#)]
55. Yanai, T.; Tew, D.P.; Handy, N.C. A new hybrid exchange–correlation functional using the Coulomb-attenuating method (CAM-B3LYP). *Chem. Phys. Lett.* **2004**, *393*, 51–57. [[CrossRef](#)]
56. Zhao, Y.; Truhlar, D.G. Density functionals with broad applicability in chemistry. *Acc. Chem. Res.* **2008**, *41*, 157–167. [[CrossRef](#)]
57. Krishnan, R.; Binkley, J.S.; Seeger, R.; Pople, J.A. Self-consistent molecular orbital methods. XX. A basis set for correlated wave functions. *J. Chem. Phys.* **1980**, *72*, 650–654. [[CrossRef](#)]
58. Tomasi, J.; Mennucci, B.; Cammi, R. Quantum mechanical continuum solvation models. *Chem. Rev.* **2005**, *105*, 2999–3094. [[CrossRef](#)]

59. Pielak, K.; Bondu, F.; Sanguinet, L.; Rodriguez, V.; Champagne, B.; Castet, F. Second-order nonlinear optical properties of multiaddressable indolinoxazolidine derivatives: Joint computational and hyper-Rayleigh scattering investigations. *J. Phys. Chem. C* **2017**, *121*, 1851–1860. [[CrossRef](#)]
60. Brasselet, S.; Zyss, J. Multipolar molecules and multipolar fields: Probing and controlling the tensorial nature of nonlinear molecular media. *JOSA B* **1998**, *15*, 257–288. [[CrossRef](#)]
61. Khan, M.U.; Ibrahim, M.; Khalid, M.; Jamil, S.; Al-Saadi, A.A.; Janjua, M.R.S.A. Quantum chemical designing of indolo [3, 2, 1-jk] carbazole-based dyes for highly efficient nonlinear optical properties. *Chem. Phys. Lett.* **2019**, *719*, 59–66. [[CrossRef](#)]
62. Mendis, B.A.S.; De Silva, K.M.N. A comprehensive study of linear and non-linear optical properties of novel charge transfer molecular systems. *J. Mol. Struct. THEOCHEM* **2004**, *678*, 31–38. [[CrossRef](#)]
63. Vijayakumar, T.; Joe, I.H.; Nair, C.P.R.; Jayakumar, V.S. Efficient  $\pi$  electrons delocalization in prospective push–pull non-linear optical chromophore 4-[N, N-dimethylamino]-4'-nitro stilbene (DANS): A vibrational spectroscopic study. *Chem. Phys.* **2008**, *343*, 83–99. [[CrossRef](#)]
64. Sun, M.; Chen, J.; Xu, H. Visualizations of transition dipoles, charge transfer, and electron-hole coherence on electronic state transitions between excited states for two-photon absorption. *J. Chem. Phys.* **2008**, *128*, 64106. [[CrossRef](#)] [[PubMed](#)]
65. De La Torre, G.; Vázquez, P.; Agullo-Lopez, F.; Torres, T. Role of structural factors in the nonlinear optical properties of phthalocyanines and related compounds. *Chem. Rev.* **2004**, *104*, 3723–3750. [[CrossRef](#)] [[PubMed](#)]
66. Choi, E.-Y.; Kim, P.-J.; Jazbinsek, M.; Kim, J.-T.; Lee, Y.S.; Gu, P.; Lee, S.W.; Kwon, O.-P. 4-Nitrophenylhydrazone Crystals with Large Quadratic Nonlinear Optical Response by Optimal Molecular Packing. *Cryst. Growth Des.* **2011**, *11*, 3049–3055. [[CrossRef](#)]
67. Lou, A.J.-T.; Marks, T.J. A twist on nonlinear optics: Understanding the unique response of  $\pi$ -twisted chromophores. *Acc. Chem. Res.* **2019**, *52*, 1428–1438. [[CrossRef](#)]
68. Oudar, J.L.; Zyss, J. Structural dependence of nonlinear-optical properties of methyl-(2, 4-dinitrophenyl)-aminopropanoate crystals. *Phys. Rev. A* **1982**, *26*, 2016. [[CrossRef](#)]
69. Sciuti, L.F.; Abegão, L.M.G.; Santos, C.H.D.D.; Cocca, L.H.Z.; da Costa, R.G.M.; Limberger, J.; Misoguti, L.; Mendonça, C.R.; De Boni, L. Modeling the First-Order Molecular Hyperpolarizability Dispersion from Experimentally Obtained One- and Two-Photon Absorption. *J. Phys. Chem. A* **2022**, *126*, 2152–2159. [[CrossRef](#)]
70. Rasool, F.; Hussain, A.; Yar, M.; Ayub, K.; Sajid, M.; Asif, H.M.; Imran, M.; Assiri, M.A. Nonlinear optical response of 9, 10-bis (phenylethynyl) anthracene mediated by electron donating and electron withdrawing substituents: A density functional theory approach. *Mater. Sci. Semicond. Process.* **2022**, *148*, 106751. [[CrossRef](#)]
71. Orr, B.J.; Ward, J.F. Perturbation theory of the non-linear optical polarization of an isolated system. *Mol. Phys.* **1971**, *20*, 513–526. [[CrossRef](#)]
72. Santos, F.A.; Abegão, L.M.G.; Fonseca, R.D.; Alcântara, A.M.; Mendonça, C.R.; Valle, M.S.; Alencar, M.; Kamada, K.; De Boni, L.; Rodrigues, J.J., Jr. Bromo- and chloro-derivatives of dibenzylideneacetone: Experimental and theoretical study of the first molecular hyperpolarizability and two-photon absorption. *J. Photochem. Photobiol. A Chem.* **2019**, *369*, 70–76. [[CrossRef](#)]
73. Day, P.N.; Nguyen, K.A.; Pachter, R. Calculation of two-photon absorption spectra of donor- $\pi$ -acceptor compounds in solution using quadratic response time-dependent density functional theory. *J. Chem. Phys.* **2006**, *125*, 94103. [[CrossRef](#)] [[PubMed](#)]
74. Pal, A.K.; Duignan, T.J.; Autschbach, J. Calculation of linear and nonlinear optical properties of azobenzene derivatives with Kohn–Sham and coupled-cluster methods. *Phys. Chem. Chem. Phys.* **2018**, *20*, 7303–7316. [[CrossRef](#)] [[PubMed](#)]
75. Patil, P.S.; Dharmaprasad, S.M.; Ramakrishna, K.; Fun, H.-K.; Kumar, R.S.S.; Rao, D.N. Second harmonic generation and crystal growth of new chalcone derivatives. *J. Cryst. Growth* **2007**, *303*, 520–524. [[CrossRef](#)]
76. Azhar, S.M.; Anis, M.; Rabbani, G.; Shirsat, M.D.; Baig, M.I.; Hussaini, S.S.; AlFaify, S.; Khan, M.A. Growth of  $\text{NH}_4\text{H}_2\text{PO}_4$  crystal in urea environment to optimize linear-nonlinear optical traits for photonic device applications. *Optik* **2019**, *185*, 1247–1252. [[CrossRef](#)]
77. Abegão, L.M.G.; Fonseca, R.D.; Santos, F.A.; Souza, G.B.; Barreiros, A.L.B.S.; Barreiros, M.L.; Alencar, M.; Mendonça, C.R.; Silva, D.L.; De Boni, L. Second- and third-order nonlinear optical properties of unsubstituted and mono-substituted chalcones. *Chem. Phys. Lett.* **2016**, *648*, 91–96. [[CrossRef](#)]
78. Abegão, L.M.G.; Santos, F.A.; Fonseca, R.D.; Barreiros, A.L.B.S.; Barreiros, M.L.; Alves, P.B.; Costa, E.V.; Souza, G.B.; Alencar, M.A.R.C.; Mendonça, C.R. Chalcone-based molecules: Experimental and theoretical studies on the two-photon absorption and molecular first hyperpolarizability. *Spectrochim. Acta Part A Mol. Biomol. Spectrosc.* **2020**, *227*, 117772. [[CrossRef](#)]

**Disclaimer/Publisher’s Note:** The statements, opinions and data contained in all publications are solely those of the individual author(s) and contributor(s) and not of MDPI and/or the editor(s). MDPI and/or the editor(s) disclaim responsibility for any injury to people or property resulting from any ideas, methods, instructions or products referred to in the content.